Environmental Engineering and Management Journal *June 2021, Vol. 20, No. 6, 883-893*
http://www.eemj.icpm.tuiasi.ro/; http://www.eemj.eu

"Gheorghe Asachi" Technical University of Iasi, Romania

TREATMENT OF PERSISTENT ORGANIC POLLUTANTS IN LED REACTOR USING FERROUS SULFATE AND IRON WASTE FOR FENTON PROCESS

Sérgio Gonzaga dos Santos Júnior[1], Rayany Magali da Rocha Santana[1], Rayssa Kelen de Mendonça Gomes[1], Nathália Farias Santos de Moraes[1], Pollyanna Michelle da Silva[2], Patrícia Maria Guedes Paiva[2], Alex Leandro Andrade de Lucena[1], Graziele Elisandra do Nascimento[1], Daniella Carla Napoleão[1*]

[1]Departamento de Engenharia Química, Centro de Tecnologia e Geociências, Universidade Federal de Pernambuco, Av. dos Economistas, s/n, Recife, PE, Brasil
[2]Departamento de Bioquímica, Centro de Ciências Biológicas, Universidade Federal de Pernambuco, Av. Prof. Moraes do Rego, s/n, Recife, PE, Brasil

Abstract

The treatment of persistent pollutants in water is a subject of numerous researches around the world. In the present work, the degradation of a mixture of textile dyes by the photo-Fenton process was investigated. This was conducted under LED radiation, which has a reduced cost, employing iron in salt and residue forms. For homogeneous and heterogeneous processes, in acid medium, the effects of the H_2O_2 and iron concentrations were evaluated. The tests demonstrated that the homogeneous process was better conducted using 100 mg.L^{-1} of H_2O_2 and 2.0 mg.L^{-1} of iron, with 98% of degradation. For the heterogeneous study, H_2O_2 and iron residue concentrations of 100 mg.L^{-1} and 0.5 g.L^{-1}, respectively, were used, obtaining a 92% of degradation. The residue used was characterized by FTIR analysis. Peaks related to the presence of Fe were observed. The kinetics of the processes were evaluated, with good adjustments to non-linear models of pseudo-first order, attaining values of linear regression greater than 0.94. Toxicity tests were carried out with seeds and bacteria. It was observed a possible formation of intermediates due to the increased toxicity for the solution treated by the heterogeneous process. Artificial neural networks were used to accurately predict the degradation of the dye mixture.

Keywords: artificial neural network, AOP, dyes, kinetic modelling, toxicity

Received: July, 2020; Revised final: September, 2020; Accepted: October, 2020; Published in final edited form: June, 2021

1. Introduction

Persistent and recalcitrant contaminants have been treated by advanced oxidation processes (AOP), which have been applied for the treatment of industrial wastewater (Ergüt et al., 2019). The AOP act by generating chemical radicals, such as the hydroxyl (HO·), which are highly reactive and interact with the organic matter present in the environment, ideally forming water, carbon, dioxide and mineral salts (Klavarioti et al., 2009). Among the main AOP, the photo-Fenton can be highlighted, which is quite efficient in the treatment of organic pollutants, such as dyes. In this type of AOP, iron acts as a reaction catalyst, where hydrogen peroxide is used as an oxidizing agent. Besides, the presence of radiation helps in the process of generating hydroxyl radicals, responsible for the treatment (Wu et al., 2018; Zhu et

* Author to whom all correspondence should be addressed: e-mail: daniella.napoleao@ufe.br; Phone: +558121268711

al., 2019). The Fenton and photo-Fenton processes can use homogeneous and heterogeneous sources of iron (Rojas-Mantilla et al., 2019). However, most of the works reported in the literature used a homogeneous source of iron, which cannot be reused (Benzaquén et al., 2017).

In turn, the use of heterogeneous photo-Fenton has some advantages, such as reduced iron precipitation and the ability to reuse the catalyst (Benzaquén et al., 2017). Allied to this, it is known that the use of the heterogeneous method appears as a good alternative since it can employ iron waste from different sources. An example is the use of iron ore residue for the treatment of effluents (Rojas-Mantilla et al., 2019), which is obtained at low costs.

In general, in the photo-Fenton process, some factors are of great influence and need to be monitored. The pH has a significant effect, since it is known that at values greater than 6 there is a tendency to form iron hydroxide. This fact is undesirable since it leads to the precipitation of the metal and decreases the efficiency of the treatment (Lastre-Acosta et al., 2019). Other important factors are the oxidant and iron concentrations since its use in inadequate conditions disfavors the oxidation process.

Some types of irradiation sources have been used in the photo-Fenton process, including incandescent and florescent (Rojas-Mantilla et al., 2019). Studies reported in the literature have made use of ultraviolet or solar radiation (Reddy and Devaraju, 2019; Santana et al., 2021) and, only recently studies consider light-emitting diode (LED) technology. This type of light source attracts attention, as it employs efficient devices at affordable prices. Also, LED devices have a service life of around 50,000 h and do not contain the element mercury, which is very polluting (Gomes et al., 2021).

Based on the understanding of all the variables involved in the process, a final analysis must be carried out. This is necessary because the degradation of organic pollutants by AOP may, in some cases, not reduce the toxicity of the matrix. With this, ecotoxicological tests with different organisms (seeds, bacteria, microcrustaceans) are carried out to guarantee that after the AOP there was no formation of toxic intermediates that can cause risks to the ecosystem (Gomes Júnior et al., 2021; Fernandes et al., 2018).

Given the above, this work studied the degradation of a mixture of textile dyes (direct black 22 (DB22), direct red 23 (DR23), direct red (DR227) and reactive blue (RB21)) through the photo-Fenton AOP with LED radiation. For this, the different sources of iron were evaluated, as well as the operational parameters in the treatment employed. In addition, the toxicity of the studied matrix was investigated before and after treatment, as well as the reaction kinetics. Finally, artificial neural networks were used to help predict the percentage of degradation using both homogeneous and heterogeneous AOP.

2. Methodology

2.1. Working solution

The aqueous working solution were composed of the textile dyes mixture DB22, DR23, DR227 and RB21 containing 15 mg.L^{-1} of each (all manufactured by Exatacor). Some information about these compounds is shown in Table 1. These dyes were analyzed in an ultraviolet-visible (UV/Vis) spectrophotometer (Thermoscientific). The quantification of the dye mixture was given at a wavelength of 508 nm, which showed maximum absorbance, as can be seen in the spectrum related in Fig. 1. It is important to note that this λ is associated with the chromophore groups of the mixture, which are responsible for the color.

Table 1. Information on textile dyes

Name	***Colour Index***	***Formula***	***Molecular weight (g·mol^{-1})***
Direct Black 22	35435	$C_{44}H_{32}N_{13}Na_3O_{11}S_3$	1083.97
Direct Red 23	29160	$C_{35}H_{25}N_7Na_2O_{10}S_2$	813.73
Direct Red 227	Not cataloged	$C_{60}H_{46}N_{16}Na_6O_{22}S_6$	1673.43
Reactive Blue 21	18097	$C_{40}H_{25}CuN_9O_{14}S_5$	1079.54

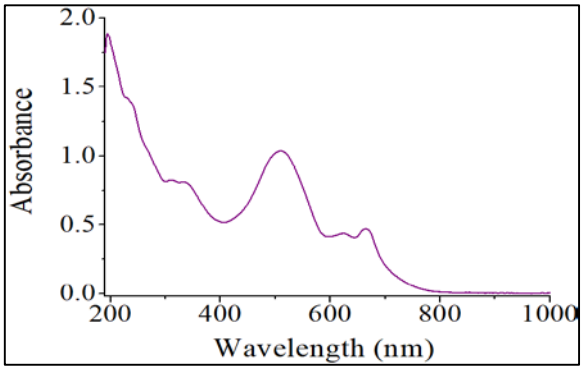

Fig. 1. UV/Vis absorption spectrum of the textile dye mixture under study

2.2. Preparation and characterization of the heterogeneous catalyst

Iron oxide (Fe_2O_3 – rust) was used as a catalyst for the reactions. Initially, the residue from equipment undergoing corrosion was macerated and subjected to three washing cycles, with 0.1 mol.L^{-1} nitric acid for 10 min; ethanol P.A. (Neon) for 10 min, and distilled water in flowing flow. After washing, the residue was dried in an oven at 100 ± 1ºC for 120 min. Once dry, with the aid of tweezers, any impurities present in the material were removed. Finally, Fe_2O_3 was sieved and classified, in Tyler sieves, in the following particle size ranges: 0.60-1.18, 0.30-0.60, 0.15-0.30 and < 0.15 mm.

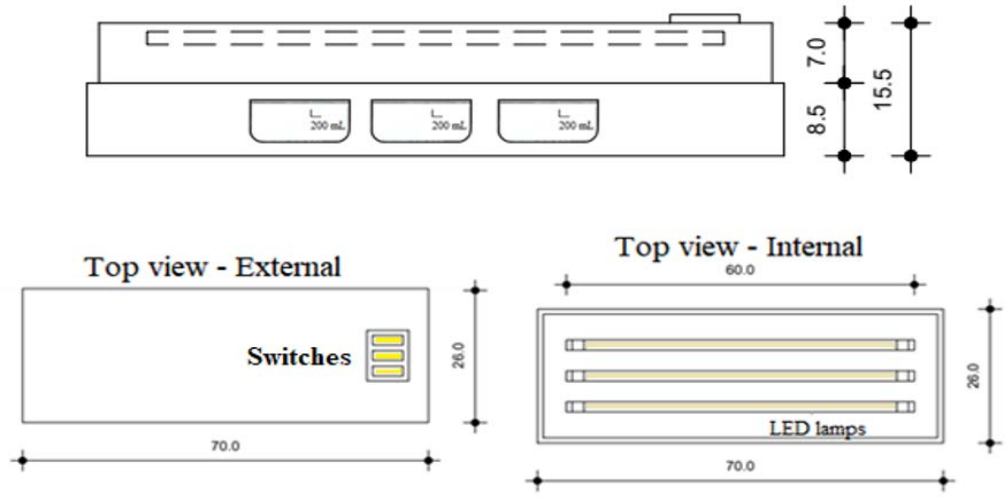

Fig. 2. Diagram of the LED bench reactor

The material was characterized by Fourier transform infrared spectroscopy (FTIR), using a Bruker Tensor 27 Equipment. The spectra were obtained in the range between 4000 to 500 cm^{-1}, with an average of 20 scans, a spectral resolution of 4 cm^{-1}, using an ATR probe.

2.3. Photo-Fenton treatment using LED reactor

A bench reactor with LED radiation was used, composed of a wooden box and 3 lamps (FLC LED) with 10 W of power each, arranged in parallel. Fig. 2 shows the schematic drawing of the reactor.

The aqueous solutions containing the mixture of textile dyes were subjected to the treatments by homogeneous and heterogeneous photo-Fenton. To analyze the efficiency of this process with a homogeneous catalyst ($FeSO_4 \cdot 7H_2O$, Vetec), univariate studies were carried out with the variables that influence the AOP. The first tests were conducted by varying the iron concentration ([Fe]) from 0.5 to 5.0 $mg.L^{-1}$. Then, 100 $mg.L^{-1}$ of hydrogen peroxide concentration ($[H_2O_2]$) were added to 200 mL of the sample, with tests done in the times of 60, 90, and 120 min. Then, with the best [Fe] determined, the $[H_2O_2]$ was varied in 40, 60, 80 and 100 $mg.L^{-1}$. For all experiments, the pH of the dye solutions was adjusted to 3. Then, and in a manner similar to that performed for the homogeneous treatment, univariate studies were carried out with the variables of the heterogeneous process. For this purpose, 200 mL of the dye solution were placed in beakers and then, initially, the pH influence on the treatment was evaluated (values of 3, 4, 5, 6 and 7). For these tests, 0.5 $g.L^{-1}$ of iron residue (< 0.15 mm) and 100 $mg.L^{-1}$ of $[H_2O_2]$ were used.

Then, the best pH was fixed, and the effect of the catalyst granulometry was evaluated. The particle sizes range analyzed were the same as previously described and the iron residue concentration ([RFe]) and $[H_2O_2]$ were kept the same as in the previous studies.

After that, the influence of the [RFe] was also evaluated (from 0.5 to 3.0 $g.L^{-1}$), followed by the $[H_2O_2]$, which was varied between 80 and 160 $mg.L^{-1}$. These tests were carried out fixing the best conditions of pH, granulometry and [RFe], for a period of 60, 120, 180 and 240 min.

2.4. Kinetic study, reuse and toxicity tests

Having established the best working conditions for the photo-Fenton / LED system using different sources of iron, the experimental data were then evaluated against the kinetic models of Chan and Chu (2003) (Eq. 1) and He et al. (2016) (Eqs. 2-4). In this stage of the study, 1000 mL of the dye solution were used on the treatments. It is important to note that the model by He et al. (2016) is described as a simplification of the Langmuir-Hinshelwood model, resulting in a pseudo-first order kinetic equation.

$$C/C_0 = 1 - t/(\rho + \sigma t) \quad (1)$$

$$-dC/dt = k_r KC/(1 + KC) \quad (2)$$

$$-dC/dt = k_r\, KC = kC \quad (3)$$

$$-\ln C/C_0 = kt \quad (4)$$

where C ($mg.L^{-1}$) is the dye concentration; C_0 ($mg.L^{-1}$) is the initial dye concentration; t (min) is the reaction time; $\frac{1}{\rho}$ (min^{-1}) and $\frac{1}{\sigma}$ (adimensional) are experimental constants that represent, respectively, the speed constant and the oxidative capacity of the system; k (min^{-1}) is the reaction rate.

The ability to reuse iron waste was determined through five consecutive degradation cycles. For this, the same conditions of the kinetic study were applied, with the efficiency determined after 540 min. Between cycles, the RFe was washed with distilled water, keeping the catalyst mass constant throughout the tests.

Before proceeding to the toxicity assessment stage, analyzes were carried out to determine residual H_2O_2, using a semi-quantitative method with a hydrogen peroxide test strip (Merck). In addition, the treated samples were neutralized so that there was no negative influence of pH on the development of the studied organisms.

For the same operational conditions, a toxicity test was carried out. This test consisted of exposing watercress (*Nasturtium officinale*), lettuce (*Lactuca sativa*) and carrot (*Daucus carota*) seeds to the solutions before and after treatment using the methodology proposed by Santos et al. (2019). At the end of the incubation, the root growth index (RGI) and the germination index (GI) were calculated, as described by Young et al. (2012). In addition to seed tests, a microbiological evaluation was also carried out, using strains of *Escherichia coli* UFPEDA 224 and *Salmonella enteritidis* UFPEDA 414, according to Gomes et al. (2021).

2.5. Artificial Neural Network Modelling

The artificial neural networks (ANN) were built using the software Statistica 6.0. Thus, it was possible to determine patterns and correlations of the experimental data for the photo-Fenton/LED system, using the two catalysts. The input variables used were: [Fe], [H_2O_2], and time for homogeneous treatment and pH, [H_2O_2], [RFe], catalyst granulometry and time for heterogeneous process, while for the output, the degradation (%) of the mixture of textile dyes was used. For the construction of the ANN, the interactions quantities were used, as well as the configuration method and the distribution of data between training, testing and validation as described by Santana et al. (2021).

3. Results and discussion

3.1. Characterization of the heterogeneous catalyst

The analysis by Fourier transform infrared spectroscopy (FTIR) allowed to investigate the functional groups present in the iron-based catalyst. The result obtained is shown in Fig. 3. From Fig. 3, it is possible to see a peak between 1000 and 1100 cm^{-1}, characteristic of the presence of iron. Kollias et al. (2019) state that the 1100 cm^{-1} band corresponds to the asymmetric elongation of silicon functional groups, such as Si-O. On the other hand, the acute peak around 1094 cm^{-1} occurs due to the vibration of the asymmetric Si-O-Si elongation, as reported by Jiang et al. (2018). These authors also stated that the wide stretch around 3453 cm^{-1}, also seen in Fig. 3, corresponds to the elongation of O-H connections.

Finally, the behavior of the spectrum observed between 1000 and 500 cm^{-1} is characteristic of the presence of Fe-O, as described by Zhang et al. (2019). This shows that the rust used presents an expected behavior for Fe_2O_3.

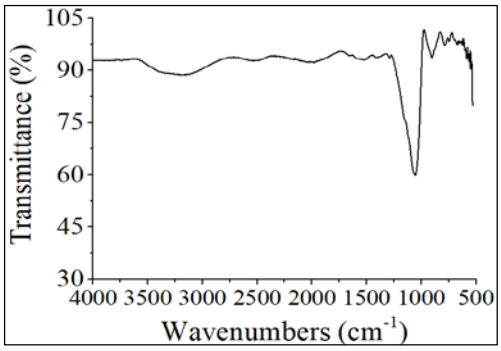

Fig. 3. Infrared absorption spectrum for the iron waste

3.2. Homogeneous photo-Fenton treatment

Initially, different iron concentrations were evaluated to obtain the best percentage of degradation of the dye. Fig. 4 shows the results obtained.

Looking at Fig. 4, it can be seen that the [Fe] that provided the best efficiency after 120 min was 5.0 $mg.L^{-1}$ (98% degradation). It is important to note that the Fenton reaction requires ferrous ions to occurs, therefore, an increase in the percentage of degradation is observed when the iron concentration in the solution is increased. However, there is a limiting concentration from which ferrous ions are harmful to the process since self-inhibition of the oxidizing ion can occur (Bensalah et al., 2019).

Thus, considering that the degradation obtained was high, it was decided not to increase the iron concentration anymore. In addition, the analysis of Fig. 4 shows a significant degradation (96%) when using 2.0 $mg.L^{-1}$ of iron. For this reason, this lower concentration was used in order to employ a smaller amount of the reagent and thus reduce operating costs.

Therefore, the [Fe] was fixed and the ideal [H_2O_2] was evaluated to guarantee a sufficient number of oxidizing radicals to treat the organic pollutant. The results obtained when using different [H_2O_2] are shown in Fig. 5.

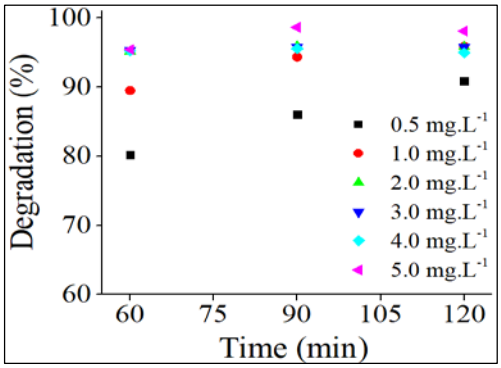

Fig. 4. Monitoring of the textile dyes mixture degradation using different [Fe]

In Fig. 5, it can be seen that the [H_2O_2] that provides the best percentage of degradation for the dye mixture under study was 100 $mg.L^{-1}$, leading to a degradation greater than 98%. It is important to note

that in these tests a degradation equal to that obtained in the previous study was achieved when 5 mg.L^{-1} of iron was used. This indicates that the 2% increase may be due to experimental errors and corroborates that a smaller amount of iron can be used without prejudice to the efficiency of the treatment.

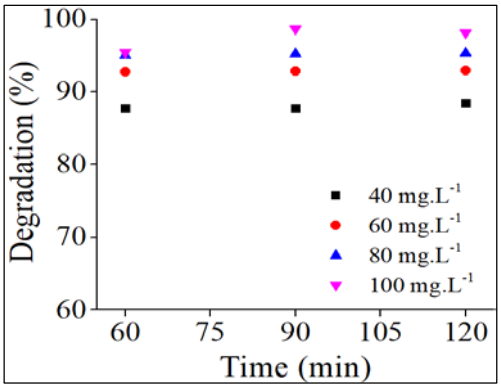

Fig. 5. Result of the textile dyes mixture degradation for different [H_2O_2]

It can also be seen that the percentage of degradation of the dye mixture increased with the increase in [H_2O_2]. Based on that, it is important to highlight that, in a manner similar to the behavior of the [Fe], there is also a limiting concentration for the [H_2O_2] (Zhang et al., 2020). However, given an almost complete degradation of the pollutant, it was decided not to increase the concentration of the oxidizing agent anymore, as it would not be economically viable and would not provide more efficient results when using the process under study.

3.3. Heterogeneous photo-Fenton treatment

Once the homogeneous treatment was carried out, the use of a heterogeneous iron source in the photo-Fenton process was studied. To this end, different pH values were tested, since heterogeneous Fenton reactions can be conducted over a larger pH range, as observed by Chen et al. (2020).

Analyzing Fig. 6, it can be seen that the highest percentage of degradation for the textile dye mixture was at pH 3.0 (≈ 92%). It is important to note that when maintaining the pH at values close to neutrality, no degradation was observed for the applied treatment. This result may indicate that the iron residue used may have released a greater amount of Fe^{3+} ions that may have precipitated (Oral and Kantar, 2019; Rubeena et al., 2018).

For a better understanding of this result, the Hydra software was used to predict the precipitation range of iron ions, as can be seen in Fig. 7.

According to Fig. 7(a), it is observed that the presence of Fe^{2+} ions leads to the formation of precipitates around pH 8. However, when there is iron oxide (Fig. 7(b)), there is the formation of iron precipitate in the entire pH range analyzed, as well as in the iron waste concentration range used (from 0.5 to 3.0 g.L^{-1}, that is, of 8.96 to 54.00 mM). Therefore, this analysis revealed that the catalyst used followed the expected pattern for Fe_2O_3, showing that the reaction using this material is favored in acidic pH.

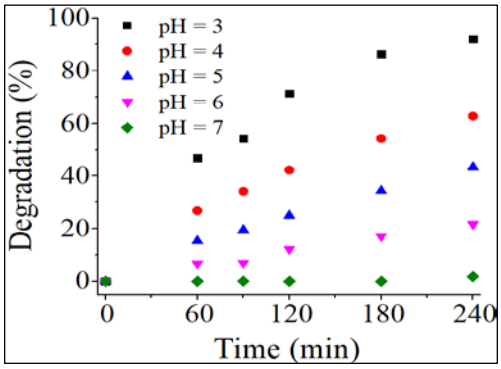

Fig. 6. Influence of pH on the degradation process of the dye mixture

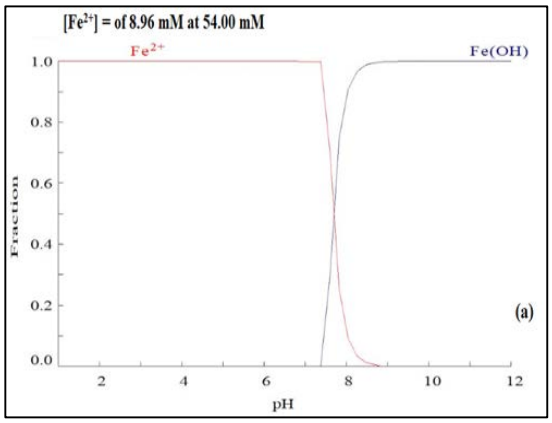

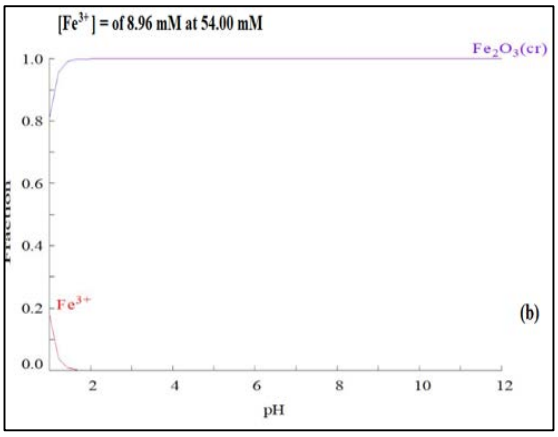

Fig. 7. (a) $Fe(OH)_2$ and Fe^{+2} ion precipitation range as a function of pH; (b) Fe_2O_3 and Fe^{+3} ions precipitation range as a function of pH

In view of the above, in the following study, the treatment continued to be conducted at pH 3, and then the influence of granulometry was evaluated (Fig. 8). As can be seen in Fig. 8, the use of the smallest particle size (<0.15 mm) led to the best results (more than 92% of degradation). Salgado and Gonzalez (2003) obtained similar results for a platinum catalyst, showing that the catalytic activity is related to the particle diameter. The authors state that the catalyst's

surface area is inversely proportional to the particle diameter, thus corroborating the results of the present study. Then, the degradation was evaluated according to different concentrations of the iron residue, with particles of diameter <0.15 mm. The results obtained are shown in Fig. 9.

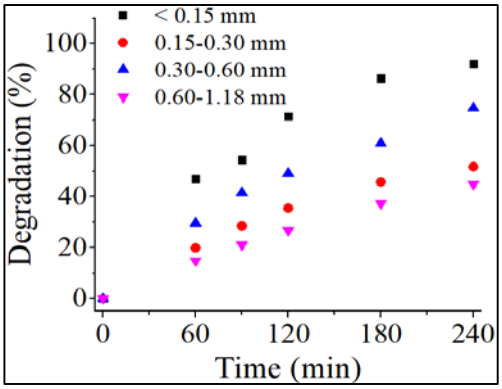

Fig. 8. Evaluation of the influence of the catalyst particle diameter on the process of degradation of the dye mixture

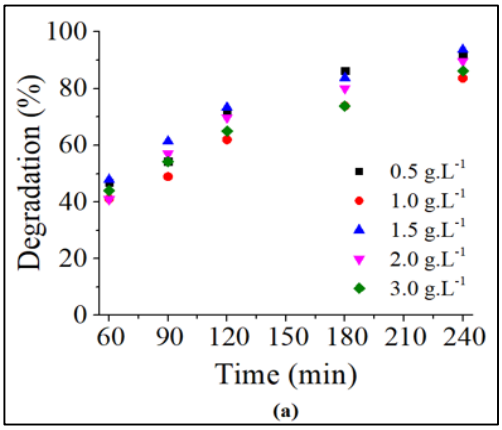

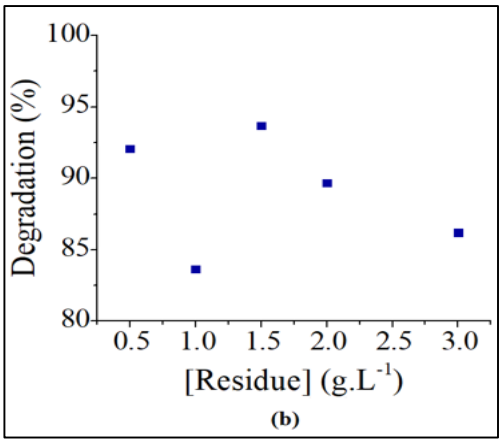

Fig. 9. Degradation of the dye mixture: (a) kinetic monitoring of the influence of iron residue concentration and (b) results after 240 min using different residue concentrations

According to what was observed in Fig. 9(a) and (b), it is noted that the [RFe] that provided the best degradation was 1.5 g.L^{-1} (93.7% of degradation). Besides, the decrease in the efficiency of the treatment with the increase in the concentration of iron residue may be associated with the fact that when using a higher metal concentration, an autoinhibition of the oxidizing radical occurs. This inhibition in turn leads to the formation of hydroxyl ions as described by Bensalah et al. (2019) (Eq. 7).

$$Fe^{2+} + HO \rightarrow Fe^{3+} + HO^{-} \quad (7)$$

However, it is possible to verify that the results obtained for 0.5 g.L^{-1} are very close (92% of degradation), with no significant difference (1.7%). Jiang et al. (2018) and Zhang et al. (2019) also used Fe_2O_3 when employing the photo-Fenton process using xenon lamps with visible radiation for the degradation of the dyes malachite green, rhodamine B, and alizarin red, respectively. Both studies achieved more than 90% efficiency. Then, the influence of [H_2O_2] in the treatment was evaluated, employing the best operational conditions found in the previous items (pH = 3.0 and 0.5 g·L^{-1} of the iron residue with granulometry < 0.15 mm). Fig. 10 shows the results obtained.

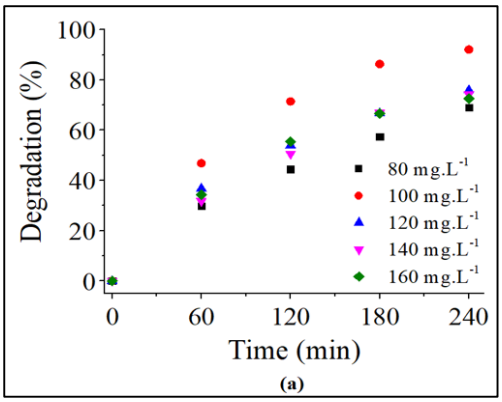

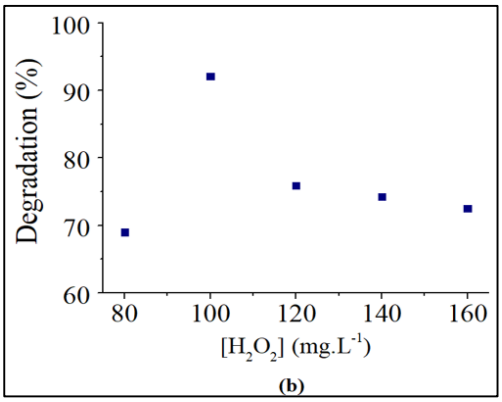

Fig. 10. (a) Evaluation of the degradation of the dye mixture by varying the concentration of H_2O_2 as a function of time; (b) Percentage of degradation for [H_2O_2] in 240 min

In Figs. 10(a) and (b) it can be seen that the limiting H_2O_2 concentration for the degradation process was 100 mg.L^{-1} (92% of degradation). It can be seen that by increasing the oxidant concentration from 80 to 100 mg.L^{-1}, there was an increase in the efficiency of the treatment, followed by a decay for the

following conditions. It is known that for the AOP to occurs, hydroxyl radicals are generated, which react with the substances thought three different mechanisms: abstraction of the hydrogen atom, electrophilic addition, and electron transfer.

However, regardless of the type of mechanism involved in the generation of the $HO^{\cdot}$ radicals, it is known that some reagents, when in excess, can disadvantage the reaction, decreasing the efficiency of the process. An example of this can be seen in Eqs. (8-9), where the excess of oxidant starts to sequester free radicals responsible for degrading organic compounds, observing the formation of the superoxide radical ($HO_2^{\cdot}$), whose reduction potential is less than the hydroxyl radicals (Galeano et al., 2019).

$$H_2O_2 + HO \rightarrow H_2O + HO_2 \quad (8)$$

$$HO_2 + HO \rightarrow H_2O + O_2 \quad (9)$$

3.4. Kinetic study and toxicity tests for homogeneous and heterogeneous AOPs

A kinetic study was carried out to observe the concentration decay over time. For this, 100 mg.L^{-1} of [H_2O_2] and 2 mg.L^{-1} of [Fe] were used for the homogeneous photo-Fenton process and 100 mg.L^{-1} of [H_2O_2] and 0.5 g.L^{-1} of [RFe] (<0.15 mm) for the heterogeneous process, with both studies being carried out at pH 3.0. Then, the kinetic models of Chan and Chu (2003) and He et al. (2016) were evaluated. Fig. 11 shows the results obtained for both treatments.

Based on Fig. 11, the experimental data adjusted well to the evaluated kinetic models. For the homogeneous study, R^2 were 0.98 and 0.94 for Chan and Chu (2003) and He et al. (2016), respectively. While for the heterogeneous treatment, R^2 = 0.99 was obtained for both models.

Analyzing the kinetic parameters obtained, it is noticed that the velocity rates ($1/\rho$ and k) for the heterogeneous treatment are lower than for the homogeneous treatment, indicating that in the first case the degradation followed a slower trend. This low reaction speed for the heterogeneous process is related to the generation of $HO^{\cdot}$ radicals, which occurred more slowly in the first minutes. This fact is related to the slow release of iron ions to the dye solution. In addition, when analyzing the parameter σ for both treatments, it is noted that the maximum oxidative capacity for the homogeneous system was also slightly higher, indicating a higher rate of degradation.

After finishing the kinetic study, the residual H_2O_2 (H_2O_2res) in each studied process was determined. It was found that for the homogeneous AOP 5 ≤ [H_2O_2] ≤ 10 mg.L^{-1}, while the heterogeneous process showed 0.5 ≤ [H_2O_2] ≤ 2 mg.L^{-1}. From the reuse study of the heterogeneous catalyst, it was found that there was no significant loss in treatment efficiency after 5 cycles, since the degradation difference was less than 1.5%. This showed the ability to reuse iron waste, which is an important and attractive feature for industrial scale application. Finally, the toxicity of the solutions was evaluated before and after treatments.

The results obtained for the germination (GI) and root growth (RGI) indices can be seen in Fig. 12. It should be noted that there was no germination of the seeds exposed to the acidic solution (positive control). When analyzing Figs. 12(a) and (b) it is noted that the GI and RGI of all the treated solutions, for all species, were lower than the negative control (N.C.), revealing the toxicity of the by-products formed after the treatment.

According to Young et al. (2012), RGI values below 0.8 indicate an inhibition of seed growth. It can also be observed that the heterogeneous treatment showed a greater inhibition potential for the development of the studied seeds when compared to the dissolved catalyst. In addition, it is observed that the solutions before the treatments showed better results than the solutions after the treatment. According to Sun et al. (2019), this is due to the presence of nutrients in the effluent composition, in particular, nitrogen. The tests using bacteria took into account the data from optical density at 600 nm (OD_{600}) and cell viability. The results obtained are shown in Table 2.

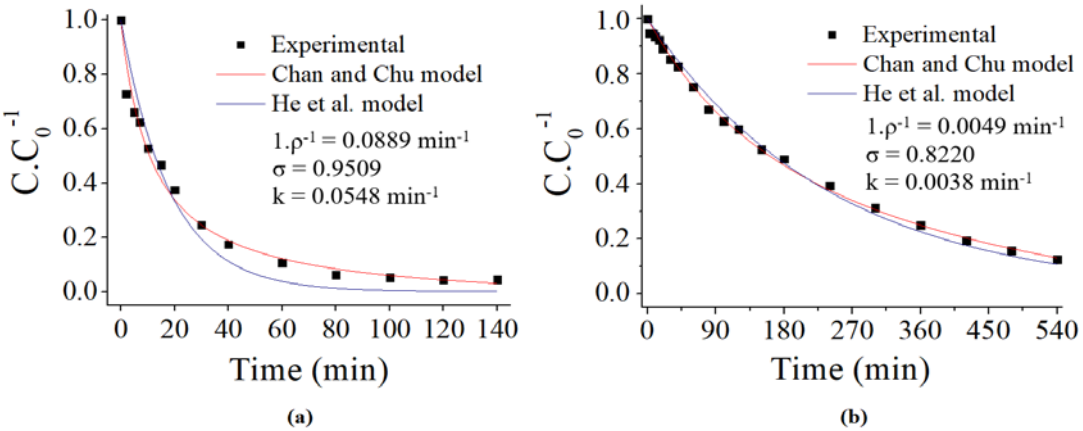

Fig. 11. Kinetic with adjustment to the models of Chan and Chu (2003) and He et al. (2016): (a) Homogeneous photo-Fenton process (b) Heterogeneous photo-Fenton process

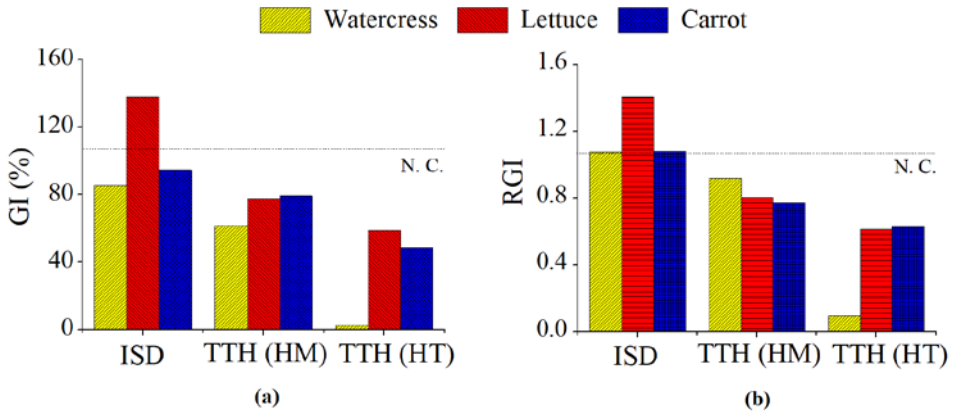

Fig. 12. Graphical analysis of the values of (a) RGI and (b) GI (%) for the initial sample of dyes (ISD) and the one treated through homogeneous (TTH_{HM}) and heterogeneous (TTH_{HT}) AOP

Table 2. Percentage of growth and cell viability of *Escherichia coli* and *Salmonella enteritidis*

Samples	t_{24h}-t_{0h} ***Mean ± σ(OD600)***		***Growth (%)***		***Viability***	
	EC	***SE***	***EC***	***SE***	***EC***	***SE***
Water (control)	0.16±0.01	0.13±0.00	100.00	100.00	+++	+++
ISD	0.27±0.02	0.26±0.05	165.21	205.82	+++++	+++++
TTH (HT)	0.00±0.00	0.02±0.00	0.20	16.13	-	+
TTH (HM)	0.17± 0.00	0.04± 0.00	104.96	35.44	+++	++

Note: EC: Escherichia coli; SE: Salmonella enteritidis; viability (+); unfeasibility (-); OD: optical density.

According to the data in Table 2, it appears that the samples treated by the heterogeneous AOP inhibited the growth of bacteria, given that the percentages of growth and viability observed were lower than those obtained for the control (water). This indicates, as with seed tests, that toxic intermediates must have been generated.

For the homogeneous treatment, the analyzes showed different results, with no evidence of toxicity for the *E. coli* and with growth inhibition for the *S. enteritidis*. In this sense, it is also important to note that residual reagents, such as iron and H_2O_2, can interfere with the results of cell viability, as well as with germination and root growth of seeds. As described by Santos et al. (2020), when carrying out tests with these reagents, it was possible to verify the inhibition of the cell viability of the studied bacteria, when in the presence of iron, however, the residual reagents did not alter the germination and root growth of seeds.

3.5. Artificial Neural Network

After verifying that there was good degradation of the dye mixture with the different AOP, a mathematical evaluation was made using an artificial neural network (ANN). Given the particularities of the homogeneous and heterogeneous processes, two distinct networks were set up. The descriptive statistics of the variables used in the ANN are contained in Table 3.Through the analysis of Table 3, it was possible to predict the maximum degradation of the dye mixture equal to 98.12% and 93.69% for the homogeneous and heterogeneous processes, respectively.

Then, followed the optimization step of the ANN topology, using a posterior propagation of three layers (3:3:1 and 5:5:1, for homogeneous and heterogeneous AOP, respectively) to model the degradation of the mixture of dyes under study. In Fig. 13, the ANN diagrams architectures MLP 3-3-1 BFGS 107 (homogeneous) and MLP 5-5-1 BFGS 205 (heterogeneous) can be seen.

In Fig. 13, it is possible to observe that the training algorithms BFGS 107 and BFGS 205, with SOS error function, presented the following activation functions: tanh and logistic for the inner layer and tanh and sine for the output layer, of the homogeneous and heterogeneous processes, respectively. The mentioned ANNs, models (3-3-1) and (5-5-1), presented values of R^2 equal to 0.997, 0.995 and 0.993 for training, testing, and validation, respectively of the homogeneous AOP and equal to 0.978; 0.978 and 0.980 for the heterogeneous treatment. Then, training, validation and test errors were determined, using an inverse interval scale to return the predicted responses to their original scale, comparing them with the experimental responses. The ANN used in this work provided the weights listed in Table 4.

The weights shown in Table 4 refer to the coefficients between the artificial neurons, so that each one decides which proportion of the received signal will be transmitted to the neuron's body. Thus, it was then possible to make comparisons between experimental and simulated results, through graphs of linear regressions, MLP (BFGS 107 and BFGS 205) for the respective, homogeneous, and heterogeneous processes studied (Fig. 14).

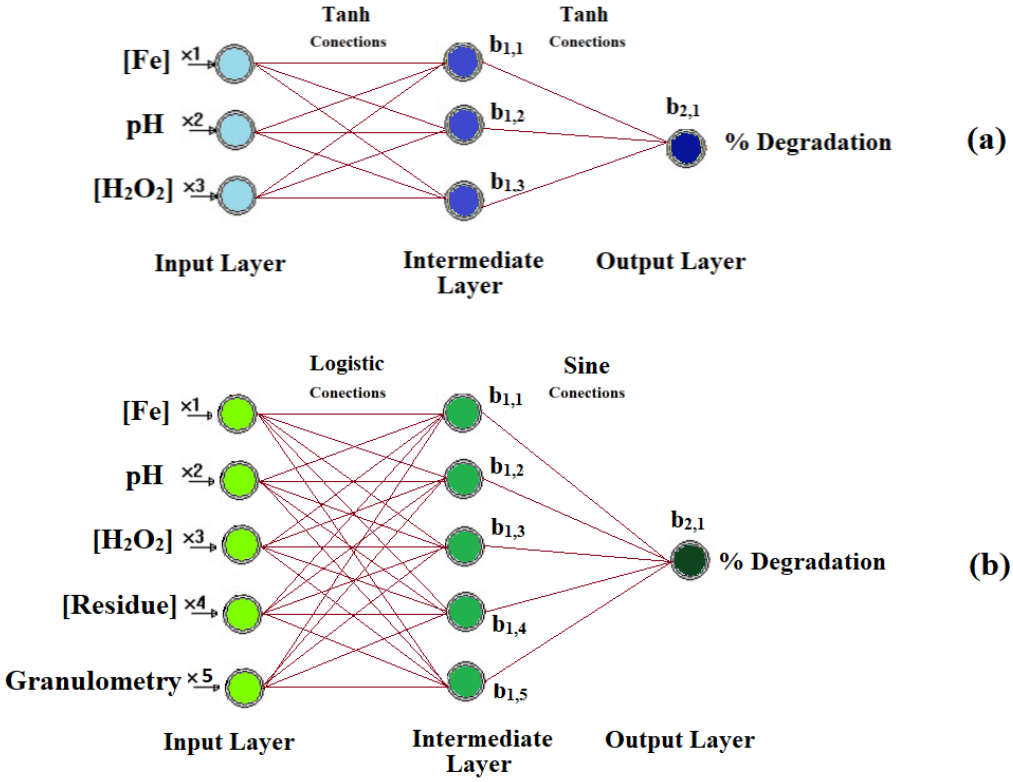

Fig. 13. ANN architecture diagram: (a) MLP 3-3-1 BFGS 107; (b) MLP 5-5-1 BFGS 205

Table 3. Descriptive statistics of the variables used in the ANN.

Variables/	*Homogeneous photo-Fenton/LED*				*Heterogeneous photo-Fenton/LED*					
	Time (min)	*H_2O_2 ($mg.L^{-1}$)*	*Fe^{2+} ($mg.L^{-1}$)*	*Degradation%*	*Time (min)*	*pH*	*H_2O_2 ($mg.L^{-1}$)*	*Residue*	*Granulometry*	*Degradation%*
Min (Tr)	2.00	40.00	0.50	27.28	2.00	3.00	80.00	0.50	14.00	0.00
Max (Tr)	120.00	100.00	5.00	98.66	540.00	7.00	160.00	3.00	100.00	93.69
Mean (Tr)	78.14	91.33	2.30	86.25	145.04	3.54	104.65	0.79	89.18	44.62
SD (Tr)	36.89	18.24	1.09	18.77	99.73	1.15	16.21	0.67	26.07	25.91
Min (Te)	10.00	40.00	1.50	47.24	5.00	3.00	80.00	0.50	14.00	0.00
Max (Te)	120.00	100.00	5.00	**98.12**	300.00	7.00	140.00	3.00	100.00	**93.69**
Mean (Te)	72.22	90.00	2.36	86.81	136.67	3.60	102.79	0.70	86.14	42.81
SD (Te)	36.87	19.70	0.94	14.37	85.96	1.33	10.31	0.50	27.99	26.18
Min (Val)	2.00	40.00	0.50	27.28	7.00	3.00	80.00	0.50	14.0	1.70
Max (Val)	120.00	100.00	5.00	95.93	480.00	7.00	160.00	3.00	100.00	93.69
Mean (Val)	68.55	93.33	2.14	82.43	147.49	3.35	103.25	0.87	91.44	50.82
SD (Val)	33.50	6.86	1.65	12.57	65.89	1.69	3.29	0.40	38.30	28.60

*Note : *Tr = train; Te = test; Val = validation.*

Table 4. Values of the weights of the input, intermediate and output layers of the ANN MLP 3-3-1 (BFGS 107, Tanh-Tanh)

Neuron	*Weights (Homogeneous photo-Fenton/LED)*					*Weights (Heterogeneous- photo-Fenton/LED)*						
	Time (min.)	*[H_2O_2] ($mg.L^{-1}$)*	*Fe^{2+} ($mg.L^{-1}$)*	*Bias entry*	*Degradation (%)*	*Time (min)*	*pH*	*[H_2O_2] ($mg.L^{-1}$)*	*Residue*	*Granulo-metry*	*Bias entry*	*Degradation (%)*
1	-0.13	-0.21	0.08	-0.45	5.82	2.71	-3.8	-7.14	3.10	16.16	-6.19	-3.03
2	-2.13	0.03	-4.40	2.23	-0.58	-3.65	-3.64	1.14	0.66	-4.54	2.96	-3.35
3	-1.58	4.32	0.44	-4.54	-2.25	5.96	-3.93	5.56	-2.91	8.64	-10.77	0.65
						0.00	-0.99	-0.26	0.48	1.08	-1.86	3.42
						-0.51	-19.37	4.53	15.79	-5.64	1.36	0.42
				Bias inter-mediate	1.48	2.52						

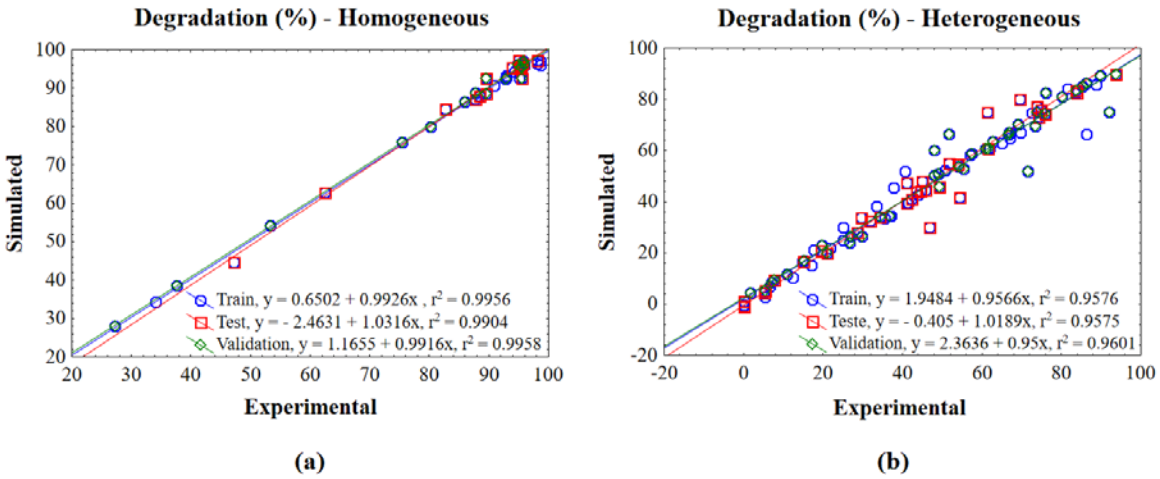

Fig. 14. Linear regressions between experimental and simulated ANN results: (a) MLP (BFGS 297) and (b) MLP (BFGS 205)

In Fig. 14, it is possible to verify a good linear correlation between the experimental and simulated results of the two networks used, with a good adaptation of the experimental data for the 3 stages (training, testing and validation). It is also possible to observe a random distribution of values, but always around the line that passes through zero.

4. Conclusions

In the studies carried out for the mixing of dyes, the use of iron residue (Fe_2O_3) in the heterogeneous photo-Fenton process allowed to reach a degradation of 92%, while the same process using a homogeneous iron source reached 98% efficiency. Besides, both procedures fit the studied models, with an accuracy greater than 94%. This indicates that the two sources of iron can be used with similar efficiency.

However, the use of iron waste allows reducing operating costs, in addition to giving a useful purpose to equipment without a function that would be discarded due to the presence of corrosion. However, through toxicity tests, growth inhibition was observed, both for watercress, lettuce and carrot seeds and for the strains of the bacteria *E. coli* and *S. enteritidis* for the heterogeneous treatment. This is indicative of a possible formation of intermediaries, making it necessary to carry out more detailed studies on the viability of the material.

Despite this, it can be said that the photo-Fenton / LED system, regardless of the type of iron used, proved to be a viable option for the degradation of the dye mixture under study. This shows that this radiation source can be applied, thus reducing energy expenditure. Finally, it was possible to use the ANN model to predict the degradation of the dye mixture. MLP-type networks managed to achieve the objective with good precision, with $R^2 \geq 0.97$.

Acknowledgments
FADE/UFPE, Núcleo de Química Analítica Avançada de Pernambuco - NUQAAPE (FACEPE, APQ-0346-1.06/14), PIBIC-UFPE/CNPq.

References

Bensalah N., Dbira S., Bedoui A., (2019), Mechanistic and kinetic studies of the degradation of diethyl phthalate (DEP) by homogeneous and heterogeneous Fenton oxidation, *Environmental Nanotechnology, Monitoring and Management*, **11**, 100224, https://doi.org/10.1016/j.enmm.2019.100224.

Benzaquén T.B., Cuello N.I., Alfano O.M., Eimer G.A., (2017), Degradation of atrazine over a heterogeneous photo-Fenton process with iron modified MCM-41 materials, *Catalysis Today*, **296**, 51-58.

Chan K.H., Chu W., (2003), Modeling the reaction kinetics of Fenton's process on the removal of atrazine, *Chemosphere*, **51**, 305-311.

Chen X.L., Li F., Chen H., Wang H., Li G., (2020), Fe_2O_3/TiO_2 functionalized biochar as a heterogeneous catalyst for dyes degradation in water under Fenton processes, *Journal of Environmental Chemical Engineering*, **8**, 1-10.

Ergüt M., Uzunoğlu D., Özer A., (2019), Efficient decolourization of malachite green with biosynthesized iron oxide nanoparticles loaded carbonated hydroxyapatite as a reusable heterogeneous Fenton-like catalyst, *Journal of Environmental Science and Health, Part A*, **54**, 786-800.

Fernandes N.C., Brito L.B., Costa G.G., Taveira S.F., Cunha Filho M.S.S., Oliveira G.A.R., Marreto R.N., (2018), Removal of azo dye using Fenton and Fenton-like processes: Evaluation of process factors by Box-Behnken design and ecotoxicity tests, *Chemico-Biological Interactions*, **291**, 47-54.

Galeano L.A., Guerrero-Flórez M., Sánchez C.A., Gil A., Vicente M.Á., (2019), *Disinfection by chemical Oxidation Methods*, In: *Applications of Advanced Oxidation Processes (AOPs) in Drinking Water Treatment*, Gil A., Galeano L.A., Vicente M.A. (Eds.), Spring, Switzerland, 257-295.

Gomes Júnior O., Santos M.G.B., Nossol A.B., Starling M.C.V., Trovó A.G., (2021), Decontamination and toxicity removal of an industrial effluent containing pesticides via multistage treatment: Coagulation-flocculation-settling and photo-Fenton process, *Process Safety and Environmental Protection*, **147**, 674-683.

Gomes R.K.M., Santana R.M.R., Moraes N.F., Santos Júnior S.G., Lucena A.L., Zaidan L.E.M.C., Elihimas D.R.M., Napoleão D.C., (2021), Treatment of direct black 22 azo dye in led reactor using ferrous sulfate and

iron waste for Fenton process: reaction kinetics, toxicity and degradation prediction by artificial neural networks, *Chemical Papers*, **75**, 1993-2005.

He Y., Sutton N.B., Rijnaarts H.H.H., Langenhoff A.A.M., (2016), Degradation of pharmaceuticals in wastewater using immobilized TiO_2 photocatalysis under simulated solar irradiation, *Applied Catalysis B: Environmental*, **182**, 132-141.

Jiang D.B., Liu X., Xu X., Zhang Y.X., (2018), Double-shell Fe_2O_3 hollow box-like structure for enhanced photo-Fenton degradation of malachite green dye, *Journal of Physics and Chemistry of Solids*, **112**, 209-215.

Klavarioti M., Mantzavinos D., Kassinos D., (2009), Removal of residual pharmaceuticals from aqueous systems by advanced oxidation processes, *Environment International*, **35**, 402-417.

Kollias K., Mylona E., Adam K., Chrysochoou M., Papassiopi N., Xenidis A., (2019), Characterization of phosphate coating formed on pyrite surface to prevent oxidation, *Applied Geochemistry*, **110**, 1-11.

Lastre-Acosta A.M., Vicente R., Mora M., Jáuregui-Haza U.J., Arques A., Teixeira A.C.S.C., (2019), Photo-Fenton reaction at mildly acidic conditions: assessing the effect of bio-organic substances of different origin and characteristics through experimental design, *Journal of Environmental Science and Health, Part A*, **54**, 711-720.

Oral O., Kantar C, (2019), Diclofenac removal by pyrite-Fenton process: Performance in batch and fixed-bed continuous flow systems, *Science of the Total Environment*, **664**, 817-823.

Reddy K.M., Devaraju J., (2019), Kinetics of photo-Fenton process and Ag-TiO_2 photocatalyst under UV-light, *Materials Today: Proceedings*, **17**, 235-238.

Rojas-Mantilla H.D., Ayala-Durán S.C., Nogueira R.F.P., (2019), Parameters affecting LED photoreactor efficiency in a heterogeneous photo-Fenton process using iron mining residue as catalyst, *Journal of Environmental Science and Health, Part A*, **54**, 1277-1286.

Rubeena K.K., Reddy P.H.P., Laiju A.R., Nidheesh P.V., (2018), Iron impregnated biochars as heterogeneous Fenton catalyst for the degradation of acid red 1 dye, *Journal of Environmental Management*, **226**, 320-328.

Salgado J.R.C., Gonzalez E.R., (2003), Relation between catalytic activity and the size of Pt / C particles prepared by different methods (in Portuguese), *Eclética Química*, **28**, 77-85.

Santana R.M., Napoleão D.C., Santos Júnior S.G., Gomes R.K.M., Moraes N.F., Zaidan L.E.M.C., Elihimas D.R.M., Nascimento G.E., Duarte M.M.B, (2021), Photo-Fenton process under sunlight irradiation for textile wastewater degradation: monitoring of residual hydrogen peroxide by spectrophotometric method and modeling artificial neural network models to predict treatment, *Chemical Papers*, https://doi.org/10.1007/s11696-020-01449-y.

Santos M.M.M., Duarte M.M.M.B., Nascimento G.E., Souza N.B.G.D., Rocha O.R.S.D., (2019), Use of TiO_2 photocatalyst supported on residues of polystyrene packaging and its applicability on the removal of food dyes, *Environmental Technology*, **40**, 1494-1507.

Santos M.M.M., Silva T.D., Lucena A.L.A., Napoleão D.C., Duarte M.M.M.B., (2020), Degradation of Ketoprofen, tenoxicam, and meloxicam drugs by photo-assisted peroxidation and Photo-Fenton processes: Identification of intermediates and toxicity study, *Water, Air, & Soil Pollution*, **231**, 1-15.

Sun D., Mullerová V., Ardestani M.M., Froutz J., (2019), Nitrogen fertilization and its legacy have inconsistent and often negative effect on plant growth in undeveloped post mining soils, *Soil & Tillage Research*, **195**, 1-9.

Wu Q., Wang H., Yi C., (2018), Preparation of photo-Fenton heterogeneous catalyst (Fe-TS-1 Zeolite) and its application in typical azo dye decoloration, *Journal of Photochemistry and Photobiology, Part A*, **356**, 138-149.

Young B.J., Riera N.I., Beily M.E., Bres P.A., Crespo D.C., Ronco A.E., (2012), Toxicity of the effluent from an anaerobic bioreactor treating cereal residues on *Lactuca sativa*, *Ecotoxicology and Environmental Safety*, **76**, 182-186.

Zhang B., Chen M., Li D., Xu H., Xia D, (2020), Quantitative investigation into the enhancing utilization efficiency of H_2O_2 catalyzed by FeOCl under visible light, *Journal of Photochemistry and Photobiology A: Chemistry*, **386**, 112072, https://doi.org/10.1016/j.jphotochem.2019.112072.

Zhang Y., Zhang N., Wang T., Huang H., Chen Y., Li Z., Zou Z., (2019), Heterogeneous degradation of organic contaminants in the photo-Fenton reaction employing pure cubic β-Fe_2O_3, *Applied Catalysis B: Environmental*, **245**, 410-419.

Zhu Y., Zhu R., Xi Y., Zhu J., Zhu G., He H., (2019), Strategies for enhancing the heterogeneous Fenton catalytic reactivity: a review, *Applied Catalysis B: Environmental*, **255**, 117739, https://doi.org/10.1016/j.apcatb.2019.05.041.